Asociación Argentina
de Mecánica Computacional

Mecánica Computacional Vol XXXI, págs. 1487-1503 (artículo completo)
Alberto Cardona, Paul H. Kohan, Ricardo D. Quinteros, Mario A. Storti (Eds.)
Salta, Argentina, 13-16 Noviembre 2012

ELASTO-PLASTIC MICROPLANE MODEL FOR FIBER REINFORCED CEMENTITIOUS COMPOSITES

Antonio Caggiano[a,b,c], Sonia M. Vrech[b], Guillermo J. Etse[a,b] and Enzo Martinelli[c]

[a]*LMNI-FIUBA, Universidad de Buenos Aires, Avda. Las Heras 2214, C1127AAR Buenos Aires, Argentina, acaggiano@fi.uba.ar*

[b]*CONICET, Universidad Nacional de Tucuman, Avda. Independencia 1800, 4000, San Miguel de Tucuman, Argentina, svrech@herrera.unt.edu.ar, getse@herrera.unt.edu.ar*

[c]*DICiv, Università degli Studi di Salerno, Via Ponte don Melillo, 84024 Fisciano, Salerno, Italy, e.martinelli@unisa.it*

Keywords: Concrete, Failure, Localization analysis, Microplanes, Plasticity.

Abstract. Quasi-brittle materials like concrete or rocks, typically present localized failure modes due to cracking processes which start from internal material defects, e.g. micro-cracks or non-homogeneous weak zones, and develop in brittle mode throughout the material. In this work both plain concrete and Fiber Reinforced Cementitious Composite (FRCC) are analyzed and modeled by means a novel microplane plasticity formulation. The continuum (smeared-crack) formulation, based on non-linear microplane theory combined with the well-known "Mixture Theory" is considered for describing the fiber effects on the failure behavior of FRCC. The interaction between cementitious matrix and steel fibers is simulated in terms of crack-bridging effect and dowel action, as similarly treated in a discontinuous model previously formulated by the authors. After describing the constitutive model, this work focuses on the numerical analysis on plain concrete and FRCC failure behavior, with particular emphasis on the fracture resistance, post-peak strength and the mechanical response related to the microplane formulation. The capabilities of the proposed model to capture the significant enhancement in the post-cracking behavior of FRCC with different fiber contents and types is finally evaluated by considering some experimental data available in scientific literature.

1 INTRODUCTION

In the latest decades, the application of Fiber-Reinforced Cementitious Composites (FRCCs) in the field of civil engineering has significantly increased. FRCC is characterized by several advantages with respect to conventional concrete. A significant residual tensile strength, accompanied with an elevate strain-energy ductility in the post-cracking regime, represents the main benefit due to the employment of FRCC in structural members (di Prisco et al., 2009).

A large amount of scientific researches were recently realized for investigating the mechanical behavior of both plain and fiber-reinforced concrete. A wide variety of models, typically based upon elastic, plastic, damage, viscous or fracture principles and formulated according to either continuous or discrete approaches, are currently available in the scientific literature (Folino and Etse (2012)). Traditional continuous models for concrete are based on the so-called Smeared Crack Approach (SCA). This kind of formulations are characterized by a significant Finite Element (FE)-mesh size dependence and the loss of ellipticity of the constitutive differential equations (Etse and Willam, 1994). Nevertheless, the main advantages of smeared crack models are related to the lower computational cost and the ease to be introduced in several commercial or open-source codes.

Discrete Crack Approach (DCA) directly consider the discontinuity of the displacement field (e.g., due to cracking) into the FE formulation. Thus, advanced numerical techniques, aimed at predicting failure behavior or crack propagation, were proposed in scientific literature within the framework of DCA. Models based on zero-thickness interfaces can be mentioned as a reference for this approach(Carol et al., 2001b; Etse et al., 2012) as well as the well-known Enriched FE (namely, E-FEM) (Oliver et al., 2006), the eXtended FE, also known as X-FEM (Meschke and Dumstorff, 2007; Liu et al., 2011), the lattice-based approaches (van Mier et al., 2002; Schauffert and Cusatis, 2012), the random particle methods (Bazant et al., 1990; Rabczuk and Belytschko, 2006), the element-free Galerkin method (Belytschko et al., 1995; Singh et al., 2011) and the hybrid-Trefftz stress-based formulation (de Freitas and Cismasiu, 2003; Kaczmarczyk and Pearce, 2009).

During the last decades, the well-known microplane theory was largely used for predicting the mechanical behavior of quasi-brittle bodies, like concrete members or soils. The pioneer works were proposed by Bazant and Gambarova (1984); Bazant and Oh (1985). Further extensions including damage and plasticity concepts were proposed in Kuhl et al. (2000); Kuhl and Ramm (2000). Other relevant microplane-based contributions can be found in the micropolar continua formulation (in the spirit of the "Cosserat media") proposed by Etse et al. (2003); Etse and Nieto (2004). Then, a nonlinear hardening-softening behavior for fiber reinforced concretes was given by Beghini et al. (2007).

The present paper formulates a novel fracture-based microplane model for simulating the failure behavior of FRCC. A normal/shear stress-crack opening formulation is considered at each microplane for describing the FRCC mechanical response and its fracture processes under normal/shear fracture modes. The general basis of the microplane assumptions are proposed in Section 2. A novel methodology to describe the composite material failure in FRCC members is given in Section 3. The well-know "Mixture Theory" by Trusdell and Toupin (1960) is taken into account therein to represent the FRCC as a composite material constituted by plain concrete matrix with fibers.

Sections 4, 5 and 7 report the constitutive laws employed at the microplane level featuring the fracture-based softening formulation for plain concrete, as well as the model description of the fiber-to-concrete interactions. Fiber-concrete interaction is explicitly considered by means

of the well known "Mixture Theory", as outlined for similar purposes by Oliver et al. (2008) and, later, by the authors Vrech et al. (2010). Both bridging- and dowel-effects of fibers which cross cracks developing in the cementitious matrix are simulated through this approach.

Finally, Section 8 presents some numerical applications of the constitutive proposal employed in microplane projections. The predictive capabilities and soundnesses of the proposal are addressed and discussed by considering several experimental results available in the scientific literature.

2 MICROPLANE BASIC ASSUMPTIONS

An elasto-plastic microplane model is proposed for simulating the macroscopic response of FRCC through a continuum smeared cracked model shown in Fig. 1. The following formulation is based on the approach given by Carol et al. (2001a) and Kuhl et al. (2001).

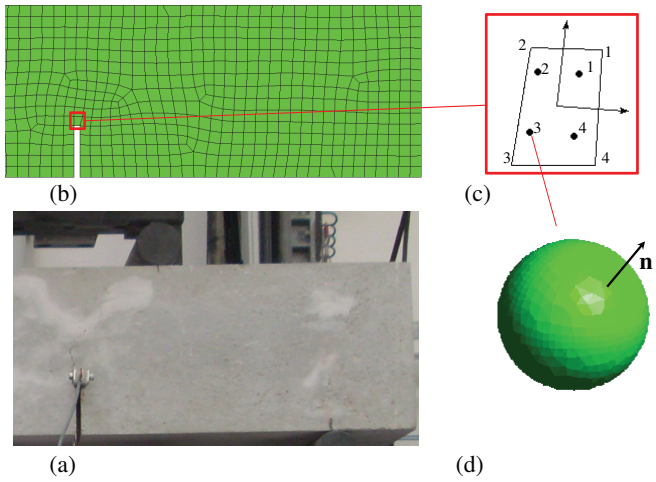

Figure 1: Geometric schematization: (a) Concrete specimen, (b) continuum discretization scale, (c) 4-node continuum FE and (d) spherical microplane region at Gauss-point with a generalized normal direction.

2.1 Kinematic assumptions

The kinematic constraint assumes that microplane normal and shear strains (ε_N and $\varepsilon_{\mathbf{T}}$, respectively) are calculated by means of the following projection relationships

$$\begin{aligned} \varepsilon_N &= \mathbf{n} \cdot \varepsilon \cdot \mathbf{n} \\ \varepsilon_{\mathbf{T}} &= \varepsilon \cdot \mathbf{n} - \varepsilon_N \mathbf{n} \end{aligned} \tag{1}$$

or in index notation

$$\begin{aligned} \varepsilon_N &= \varepsilon_{ij} n_i n_j \\ \varepsilon_{T_k} &= \varepsilon_{kj} n_j - \varepsilon_N n_k \end{aligned} \tag{2}$$

being ε the macroscopic strain tensor (ε_{ij} in index notation) projected on the microplane direction, $\mathbf{n}$ (with n_i in index notation).

2.2 Macro/microplane homogenization of stresses

The equilibrium between micro- and macroscopic stress tensor can be imposed through the Principle of Virtual Work applied in the spherical microplane region (Carol et al., 2001a)

$$\frac{4\pi}{3}\sigma_{ij}\delta\varepsilon_{ij} = 2\int_{\Omega}(\sigma_N\delta\varepsilon_N + \sigma_{T_r}\delta\varepsilon_{T_r})\mathrm{d}\Omega \tag{3}$$

where σ_{ij} denotes the components of the macroscopic stress tensor while Ω is the boundary surface of one micro-hemisphere.

Then, the following relationship for the macroscopic stress tensor can be derived by combining Eqs. (2) and (3),

$$\sigma_{ij} = \frac{3}{2\pi}\int_{\Omega}\left(\sigma_N n_i n_j + \frac{\sigma_{T_k}}{2}\left[n_i\delta_{kj} + n_j\delta_{ki}\right]\right)\mathrm{d}\Omega \tag{4}$$

where σ_N and σ_{T_k} are the microplane components of stress in the normal and tangential directions, respectively.

3 FRCC COMPOSITE FORMULATION

A smeared cracked microplane model for FRCC, based on the well-known "Mixture Theory" Trusdell and Toupin (1960), is formulated by means of the composite combination of three internal constitutive laws, whose main features are detailed between Sections 4 to 7.

Fiber reinforced concrete is assumed to be a composite constituted by a mortar matrix reinforced by randomly oriented fibers. According to the basis of the "Mixture Theory", it can be considered that each infinitesimal volume (of the continuum composite) is simultaneously occupied by all constituents. It follows that the corresponding composite stress field is given by the weighted sum (in terms of the volume fraction) of the constituent stresses

$$\sigma = w(\rho_m)\sigma^{mic} + \sum_{f=0}^{n_f} w(\rho_f)\left[\sigma_f\left(\varepsilon_N\right)\mathbf{n} + \tau_f\left(\varepsilon_{\mathbf{T}}\right)\mathbf{t}\right] \tag{5}$$

being $w(\rho_{\#})$ the weighting functions defined in Caggiano et al. (2012a), which are based on the volume fraction of each constituent $\rho_{\#}$; m and f are indices dealing with the mortar and fiber, respectively; σ_f and τ_f are related to bond-slip response and dowel action of the single fiber; they are related to the axial and tangential fiber strains, ε_N and $\varepsilon_{\mathbf{T}}$, respectively; n_f represents the number of fibers per microplane and finally, $\mathbf{n}$ and $\mathbf{t}$ are the fiber direction and its orthogonal (assumed equal to the microplane direction), respectively.

4 FRACTURE ENERGY-BASED MICROPLANE MODEL FOR PLAIN CONCRETE

The inelastic model for plain concrete failure behavior is proposed in this section. A detailed description of the microplane-based elasticity and post-peak formulation is given in the following.

4.1 Microplanes and elasto-plasticity

The microplane components of stress, σ_N and σ_{T_k} are obtained as follows from the microscopic free-energy potential, ψ_0^{mic}

$$\sigma_N = \frac{\partial\left[\rho_0\psi_0^{mic}\right]}{\partial\varepsilon_N}, \qquad \sigma_{T_k} = \frac{\partial\left[\rho_0\psi_0^{mic}\right]}{\partial\varepsilon_{T_k}} \tag{6}$$

where ρ_0 is the material density.

The macroscopic free-energy potential per unit mass in isothermal conditions can be denoted as $\psi_0^{mac}(\varepsilon, \kappa)$, where κ is a set of thermodynamically consistent internal variables; it can be expressed as follows:

$$\psi_0^{mac} = \frac{3}{2\pi} \int_{\Omega} \psi_0^{mic} \left(\varepsilon^{mic}, \kappa^{\mathbf{mic}}\right) \mathrm{d}\Omega \tag{7}$$

being ε^{mic} the vector collecting the normal and shear strain components for the microplane and $\kappa^{\mathbf{mic}}$ the vector of the internal microplane variables for accounting the hardening/softening material behavior.

Fully uncoupled normal/tangential material laws are defined at microplane level. The normal and tangential stress components are given as conjugate components of the corresponding microplane strains, i.e.,

$$\sigma_N = \frac{\partial \psi_0^{mic}}{\partial \varepsilon_N^{el}} \qquad \dot{\sigma}_N = E_N \left[\dot{\varepsilon}_N - \dot{\varepsilon}_N^p\right], \tag{8}$$

$$\sigma_{T_k} = \frac{\partial \psi_0^{mic}}{\partial \varepsilon_{T_k}^{el}} \qquad \dot{\sigma}_{T_k} = E_T \left[\dot{\varepsilon}_{T_k} - \dot{\varepsilon}_{T_k}^p\right]. \tag{9}$$

where E_N and E_T are the microscopic elastic stiffnesses.

In analogy to the macroscopic plasticity, the constitutive formulation is herein introduced in incremental form. The additive decomposition into the elastic and plastic contributions takes place in both normal (Eq. 8) and tangential strains (Eq. 9).

$\mathbf{C}^{mic}$ matrix arrays the elastic stiffness operators which connect the incremental stress rate vector, $\dot{\sigma}^{mic}$, with the rate of the microplane elastic strains $\dot{\varepsilon}^{el,mic}$

$$\mathbf{C}^{mic} = \begin{pmatrix} E_N & 0 & 0 \\ 0 & E_T & 0 \\ 0 & 0 & E_T \end{pmatrix}; \quad \dot{\sigma}^{mic} = \mathbf{C}^{mic} \cdot \dot{\varepsilon}^{el,mic}. \tag{10}$$

The microscopic elastic moduli are related to the macroscopic ones (Bazant and Prat, 1988a,b) by analytically integrating the projection of four-order tensor products as follows

$$E_N = 3K + 2G \qquad E_T = 2G \tag{11}$$

being K and G the Bulk and shear macroscopic moduli, respectively.

4.2 Post-cracking behavior

The inelastic behavior is described at microplane level by evaluating the normal/shear stress vs. strain relationship with the aim to characterize the non-linear fracture of concrete behavior.

Table 1 outlines the main laws of the microplane theory for plain concrete material. As in classical plasticity, the model starts with the microplane strain decomposition into elastic and plastic components: $\dot{\varepsilon}^{el,mic}$ and $\dot{\varepsilon}^{p,mic}$, respectively.

The three-parameter hyperbola defined by Carol et al. (1997) is considered as failure surface $f\left(\dot{\sigma}^{mic}, \dot{\kappa}^{mic}\right)$ (Fig. 2). Its expression at the microplane stress-space depends on three material parameters: the tensile strength χ^{mic}, the cohesion c^{mic} and the internal friction angle ϕ^{mic}.

The plastic flow is represented by a general non-associated law defining the direction of inelastic strains, $\mathbf{m}^{mic}$, by means of the transformation operator, $\mathbf{A}^{mic}$, applied to the normal flow direction, $\mathbf{n}^{mic} = \frac{\partial f}{\partial \sigma^{\mathbf{mic}}} = \left[\frac{\partial f}{\partial \sigma_N}, \frac{\partial f}{\partial \sigma_T}\right]^t$.

Table 1: Microplane constitutive relationships for plain concrete/mortar.

	Fracture energy − based microplane model
Free energy	$\psi_0^{mac} = \frac{3}{2\pi}\int_{\Omega}\psi_0^{mic}\left(\varepsilon^{mic},\kappa^{\mathbf{mic}}\right)\mathrm{d}\Omega$ $\sigma^{\mathbf{mic}} = \frac{\mathbf{3}}{\mathbf{2\pi}}\int_{\mathbf{\Omega}}\left(\frac{\partial[\rho_0\psi_0^{\mathbf{mic}}]}{\partial\varepsilon_{\mathbf{N}}}\mathbf{N} + \frac{\partial[\rho_0\psi_0^{\mathbf{mic}}]}{\partial\varepsilon_{\mathbf{T}}}\cdot\mathbf{T}\right)\mathbf{d\Omega}$ $**$
Constitutive equation	$\dot{\sigma}^{mic} = \mathbf{C}^{mic}\cdot\left(\dot{\varepsilon}^{mic} - \dot{\varepsilon}^{p,mic}\right)$ $\dot{\varepsilon}^{mic} = \dot{\varepsilon}^{el,mic} + \dot{\varepsilon}^{p,mic}$
Yield condition	$f\left(\dot{\sigma}^{mic},\dot{\kappa}^{mic}\right) = \|\sigma_T\|^2 - [c^{mic} - \sigma_N\tan(\phi^{mic})]^2 + [c^{mic} - \chi^{mic}\tan(\phi^{mic})]^2$
Plastic Flow rule	$\dot{\varepsilon}^{p,mic} = \dot{\lambda}\mathbf{m}^{mic}$ $\mathbf{m}^{mic} = \mathbf{A}^{mic}\cdot\mathbf{n}^{mic}$
Fracture work evolution	$\dot{\kappa}^{mic} = \dot{w}_{cr}$ $\dot{w}_{cr} = \sigma_N\cdot\dot{\varepsilon}_N^p\cdot l_{cs}^I + \sigma_{T,k}\cdot\dot{\varepsilon}_{T,k}^p\cdot l_{cs}^{II}$ if $\sigma_N \geq 0$ $\dot{w}_{cr} = \sigma_{T,k}\cdot\dot{\varepsilon}_{T,k}^p\cdot l_{cs}^{II}\left(1 - \frac{\|\sigma_N\|tan(\phi^{mic})}{\|\sigma_T\|}\right)$ if $\sigma_N < 0$
Evolution laws	$p_i^{mic} = \left[1 - \left(1 - r_p^{mic}\right)S(\xi_{p_i^{mic}})\right]p_{0i}^{mic}$
Kuhn − Tucker loading conditions	$\dot{\lambda} \geq 0, \quad f\left(\dot{\sigma}^{mic},\dot{\kappa}^{mic}\right) \leq 0, \quad \dot{\lambda}\,f\left(\dot{\sigma}^{mic},\dot{\kappa}^{mic}\right) = 0$
$** N_{ij} = n_i n_j$	$T_{ijk} = \frac{1}{2}\left[n_j\delta_{ki} + n_k\delta_{ji} - 2n_j n_k n_i\right]$

Two main fracture mechanisms govern the post-cracking evolution: the mode I type of fracture reached along the horizontal axis of the failure criterion and the asymptotic Mode II type of fracture (namely IIa) characterized by shear fracture modes with very high compression stress. The ratio between the deformation work spent in fracture, w_{cr}, and the corresponding fracture energy parameters, G_f^I and G_f^{IIa}, defines a scaling parameter, $S\left[\xi_{p_i^{mic}}\right]$ by Carol et al. (1997).

The non-dimensional variable $\xi_{\#} = \xi_{p_i^{mic}}\left[w_{cr}/G_f^{\#}\right]$, outlined in Table 1, introduces the influence of the ratio between current the inelastic work spent and the available fracture energies

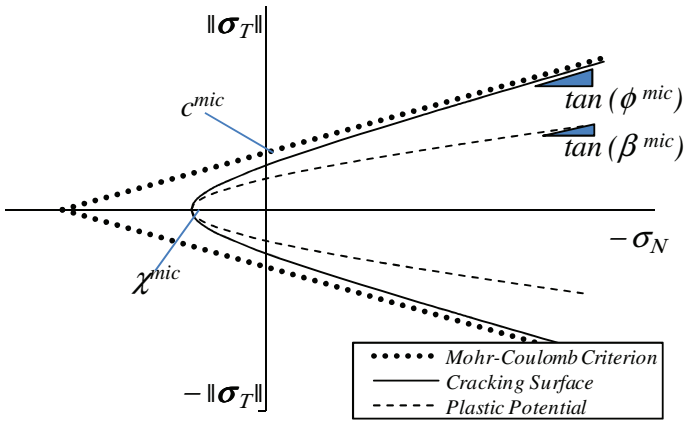

Figure 2: Maximum strength criterion by Carol et al. (1997), plastic flow rule and Mohr-Coulomb yield criterion.

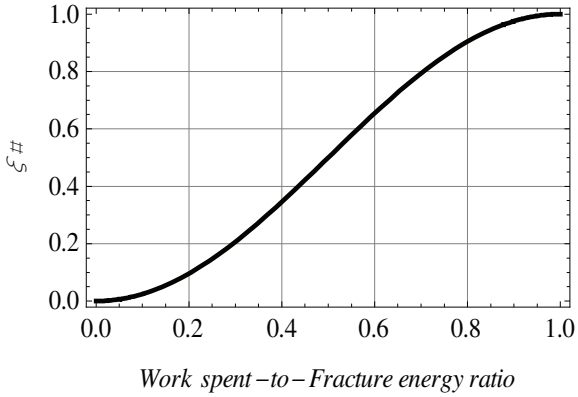

Figure 3: $\xi_\#$ functions, with $\# = \chi^{mic}, c^{mic}$ or $\tan(\alpha^{mic})$, depending on the deformation work spent-to-fracture energy ratio w_{cr}/G_f^I or w_{cr}/G_f^{IIa}.

$$\xi_{\chi^{mic}} = \begin{cases} \frac{w_{cr}}{G_f^I} & \text{if } w_{cr} \leq G_f^I \\ 1 & \text{otherwise} \end{cases} \tag{12}$$

$$\xi_{c^{mic}} = \xi_{\tan(\phi^{mic})} = \begin{cases} \frac{w_{cr}}{G_f^{IIa}} & \text{if } w_{cr} \leq G_f^{IIa} \\ 1 & \text{otherwise} \end{cases} \tag{13}$$

according to the function proposed in Carol et al. (1997). Fig. 3 shows typical curves obtained for Eqs. (12) or (13).

The expressions $\dot{w}_{cr}$, defining the rate of work spent in "mode I" and/or "II" of fracture, are based on the assumption that the components of the microplane strain vector, $\varepsilon^{\mathbf{mic}} = [\varepsilon_{\mathbf{N}}, \varepsilon_{\mathbf{T_1}}, \varepsilon_{\mathbf{T_2}}]^{\mathbf{t}}$, can easily be transformed in terms of crack-opening displacements through the following expressions

$$\varepsilon_N = \frac{u}{l_{cs}^I} \qquad \varepsilon_{T_1} = \frac{v_1}{l_{cs}^{IIa}} \qquad \varepsilon_{T_2} = \frac{v_2}{l_{cs}^{IIa}} \tag{14}$$

where u, v_1 and v_2 are relative crack displacements, while l_{cs}^I and l_{cs}^{IIa} are homogenization characteristic lengths for failure modes "I" and "II", respectively. These lengths mainly represent the crack spacing in direct tension and in shear stress states with very high confinement, respectively. Further details about the crack spacing characterization are given in Section 6.

In principle, the adopted inelastic model, its evolution laws and flow rule are similar to those already proposed by the authors in previous contributions for discrete crack analyses at material and meso-scale level Caggiano et al. (2011, 2012a).

5 CRACK-BRIDGING EFFECT AND BOND-SLIP BEHAVIOR OF FIBERS

Tensile axial stresses in fibers induced by the concrete fracture process results in relevant bridging effects. However, such a bridging effect is significantly influenced by the bond mechanisms arising between the lateral surface of fibers fibers and the concrete matrix.

As a matter of principle, the axial (tensile) stress at microplanes σ_f of a single fiber, can be derived by equilibrium conditions of shear stresses throughout the lateral contact surfaces of fibers embedded within the concrete matrix τ_a. Under these simplified assumptions a local equilibrium condition can be written on the fiber surface:

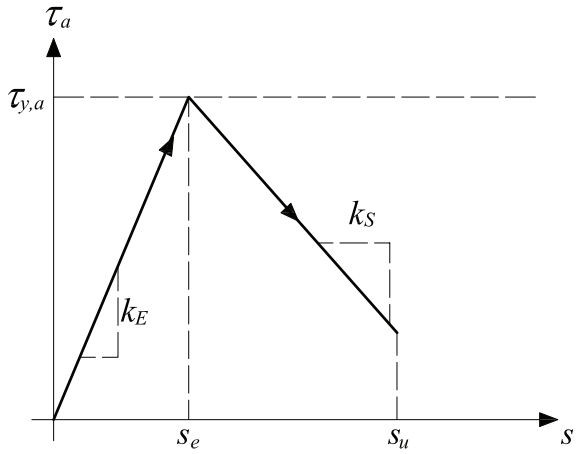

Figure 4: Bond-slip relationship with bilinear softening.

$$\frac{d\sigma_f(x)}{dx} = -\frac{4\tau_a(x)}{d_f} \tag{15}$$

where $\sigma_f(x)$ is the axial tensile stress while $\tau_a(x)$ the local bond stress between fiber and surrounding concrete, both at the point of the abscissa x; d_f represents the fiber diameter. Moreover, the present model is based on the assumption that the fibers cross fracture planes at their mid-point $l_{emb} = l_f/2$. Then, the fiber-to-concrete slip is obtained by multiplying the axial strain with the fiber length, $s(x) = \varepsilon_N \cdot l_f$. Fully elastic behavior of fibers and concrete is assumed. This is strictly true in case of synthetic fibers, while can be accepted for steel ones when the length l_{emb} satisfies the condition $\sigma_f(x) \leq \sigma_{y,s} \forall x \in [-l_{emb}, 0]$, being $\sigma_{y,s}$ the fiber yielding stress.

Under these condition it follows

$$\frac{ds(x)}{dx} = \varepsilon_c - \varepsilon_f = \frac{\sigma_c(x)}{E_c} - \frac{\sigma_f(x)}{E_f} \tag{16}$$

being $s(x)$ the debonded displacement between the fiber and concrete, ε_c and ε_f the axial strains of the surrounding concrete and fibers, E_c and E_f define the elastic moduli for concrete and fibers, respectively, while $\sigma_c(x)$ the concrete axial stress.

In each fiber cross-section, the global equilibrium condition can be defined as follows

$$N_f(x) = \sigma_c(x)A_c + \sigma_f(x)A_f \tag{17}$$

where A_c and A_f are the cross-sectional areas of the surrounding concrete and the single fiber, respectively.

Assuming a constant value of the axial resultant N_f along the x abscissa (Fantilli et al., 2009) and deriving the above equation respect to x, it can be obtained the following relationship

$$\frac{d\sigma_c(x)}{dx} = -\rho_f \frac{d\sigma_f(x)}{dx} \tag{18}$$

representing $\rho_f = A_f/A_c$ the fiber content.

Substituting Eqs. (18) and (16) into Eq. (15), the following differential equation, in terms of $s(x)$, can be achieved

$$\frac{d^2s(x)}{dx^2} + \frac{4\tau_a(x)}{d_f}\left[\frac{1}{E_f} + \frac{\rho_f}{E_c}\right] = 0 \tag{19}$$

which gives the general governing differential equation of the bonded joint between fiber and concrete which can be integrated assigning the local shear stress-slip laws defined by means of a bilinear shear-slip relationship, proposed to characterize the fiber-to-concrete debonding, which are given as follows

$$\tau_a(x) = \begin{cases} -k_E s(x) & s(x) \leq s_e \\ -\tau_{y,a} + k_S\left(s(x) - s_e\right) & s_e < s(x) \leq s_u \\ 0 & s(x) > s_u \end{cases} \tag{20}$$

where the stiffness constants $k_E \geq 0$ and $k_S \geq 0$ represent the elastic and softening slopes of such bond-slip relationships (Fig. 4), respectively; $\tau_{y,a}$ is the shear strength while s_e and s_u are the elastic and ultimate slips, respectively.

Details about the closed-form bond-slip characterization and its dissipative mechanism are not essential for the present work. The complete derivation of this numerical model and its validation against bond-slip experimental tests on FRCC but also for FRP-to-concrete bonded joints in simple shear tests, are proposed in previous works published by the authors, see Caggiano and Martinelli (2012) and Caggiano et al. (2012b) respectively.

6 CRACK SPACING

Post-cracking tension of FRCC is characterized by strain-softening behavior and the development of several cracks before the occurring of the complete failure, once the tensile strain localizes and the sample fails with only one macrocrack (Li and Leung, 1992).

Based on the original proposal by Fantilli et al. (2009), a closed-form model is proposed aimed at investigating the multiple cracking and the condition of strain-hardening behavior in High-Performance-FRCC.

6.1 FRCC strain-hardening behavior and crack distribution

Bond-slip mechanism between fibers and surrounding concrete plays a fundamental role during the post-cracking response of FRCC and, in the present model, controls the crack spacing.

Similar assumptions are considered in models for tension-stiffening behavior of concrete frames reinforced with steel bars (Nayal and Rasheed, 1992) or externally bonded by fiber-reinforced polymers (Sato and Vecchio, 2003).

Fiber is ideally considered as a reinforcement surrounded by a concrete area $A_c = A_f/\rho_f$ as shown in Fig. 5, being A_f and ρ_f the cross-sectional area and fiber content, respectively.

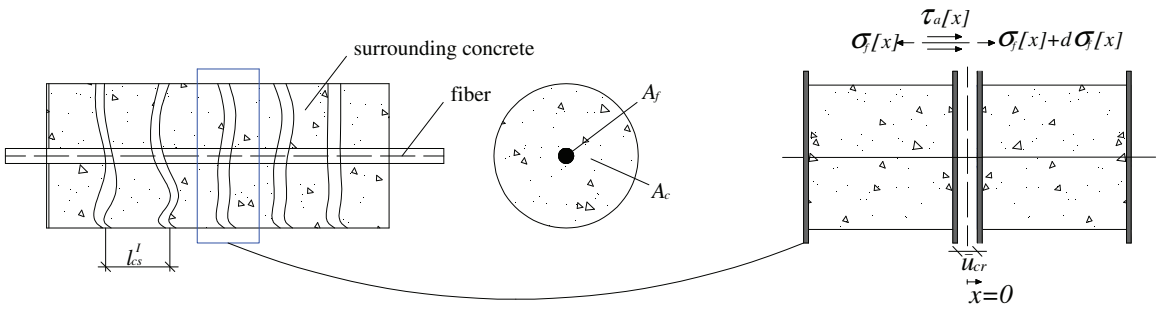

Figure 5: Equivalent strain-hardening FRCC tie in tension.

The classical solution for the tension-stiffening problem is given by the linear differential equation outlined in Eq. (19) governing the bond-slip mechanism. The conditions of multiple

cracks and strain-hardening behavior is achieved only when elastic bond mechanism is activated (Fantilli et al., 2009).

The simulation of the tension-stiffening effect in FRCC is obtained by integrating the Eq. (19), whose solution can be achieved by imposing the following boundary conditions

$$\begin{cases} s(0) = \bar{u}_{cr}/2 \\ s(l_{tr}) = 0 \end{cases} \tag{21}$$

being $\bar{u}_{cr}/2$ the half of crack width and l_{tr} the transmission length at which the slip between concrete and fiber becomes null. Then, the solution in terms of slip $s(x)$ is

$$s(x) = \frac{1}{2}\frac{\sinh\left(\alpha_1[l_{tr} - x]\right)}{\sinh\left(\alpha_1 l_{tr}\right)}\bar{u}_{cr}. \tag{22}$$

being $\alpha_1 = 2\left(\frac{k_E}{d_f}\left[\frac{1}{E_f} + \frac{\rho_f}{E_c}\right]\right)^{1/2}$.

Once the slip $s(x)$ is derived, the stress distribution in both concrete and fiber can be obtained. Particularly, the following relationship for $\sigma_c(x)$ can be calculated by substituting Eq. (15) into Eq. (18) with $\tau_a(x) = -k_E s(x)$

$$\frac{d\sigma_c(x)}{dx} = \frac{2k_E\bar{u}_{cr}\rho_f \sinh\left(\alpha_1[l_{tr} - x]\right)}{d_f \sinh\left(\alpha_1 l_{tr}\right)} \tag{23}$$

and integrating the above equation

$$\sigma_c(x) = C_1 - \frac{2k_E\bar{u}_{cr}\rho_f \cosh\left(\alpha_1[l_{tr} - x]\right)}{\alpha_1 d_f \sinh\left(\alpha_1 l_{tr}\right)}. \tag{24}$$

The integration constant C_1 can be determined by imposing the stress-crack opening relationship at crack surface, $\sigma_{cr}(\bar{u}_{cr}) = \sigma_c(x = 0)$:

$$C_1 = \sigma_{cr}(\bar{u}_{cr}) + \frac{2k_E\bar{u}_{cr}\rho_f \coth\left(\alpha_1 l_{tr}\right)}{\alpha_1 d_f} \tag{25}$$

In case of multiple cracking the tensile stress at l_{tr} equals the concrete tensile strength, $\sigma_c(x = l_{tr}) = \chi_0$. Under this condition and substituting Eq. (25) into (24)

$$\chi_0 = \sigma_{cr}(\bar{u}_{cr}) + \frac{2k_E\bar{u}_{cr}\rho_f \tanh\left(\frac{\alpha_1 l_{tr}}{2}\right)}{\alpha_1 d_f} \tag{26}$$

Finally, solving Eq. (26) for the transmission length, l_{tr},

$$l_{tr} = -\frac{2\coth^{-1}\left(\frac{2k_E\bar{u}_{cr}\rho_f}{\alpha_1 d_f[\sigma_{cr}(\bar{u}_{cr}) - \chi_0]}\right)}{\alpha_1} \tag{27}$$

According to Fantilli et al. (1998), the average crack spacing l^I_{cs} in tension for strain-hardening FRCCs assumes a value which belongs to the range $[l_{tr}, 2 \cdot l_{tr}]$. In this work the crack spacing l^I_{cs} under pure "mode I" of fracture is assumed equal to

$$l^I_{cs} = 1.5 \cdot l_{tr} \tag{28}$$

whose assumption is largely accepted in literature (Dupont and Vandewalle, 2003; di Prisco et al., 2009) and it is employed within the microplane material model of Table 1.

6.2 Critical fiber volume fraction and localized strain softening response

In case of high fiber content multiple cracking and strain-hardening behavior characterize the mechanical response of the so-called High Performance FRCC. Similar to the works by Fantilli et al. (2009), a critical value of fiber volume fraction, $\rho_{f,cr}$, outlining the boundary between strain-hardening vs. single-crack localized FRCC, can be defined by imposing the condition of infinity for the transmission length of the Eq. (27)

$$l_{tr} \to \infty; \quad \tanh\left(\frac{\alpha_1 l_{tr}}{2}\right) \to 1; \quad \chi_0 \to \sigma_{cr}(\bar{u}_{cr}) + \frac{2k_E \bar{u}_{cr} \rho_{f,cr}}{\alpha_1 d_f} \tag{29}$$

and

$$\rho_{f,cr} = \alpha_1 d_f \frac{\chi_0 - \sigma_{cr}(\bar{u}_{cr})}{2k_E \bar{u}_{cr}} \tag{30}$$

and substituting $\alpha_1 = 2\left(\frac{k_E}{d_f}\left[\frac{1}{E_f} + \frac{\rho_f}{E_c}\right]\right)^{1/2}$ in the above relation, the following relation for $\rho_{f,cr}$ can be derived (only the positive solution with physical meaning of a quadratic equation is reported)

$$\rho_{f,cr} = \frac{2\sqrt{d_f} E_c(\chi_0 - \sigma_{cr})}{\sqrt{E_f}\sqrt{d_f E_f(\chi_0 - \sigma_{cr})^2 + 4{E_c}^2 k_E \bar{u}_{cr}^2} + \sqrt{d_f} E_f(\sigma_{cr} - \chi_0)} \tag{31}$$

It is worth noting that the critical volume fraction mainly depends on the fiber material (diameter d_f and elastic modulus E_f), the surrounding concrete kind (tensile strength χ_0 and elastic modulus E_c), the crack width $\bar{u}_{cr}$ and its corresponding stress opening value σ_{cr}.

Multiple cracking, having the crack spacing $l_{cs}^I = 1.5 l_{tr}$, and strain-hardening response is obtainable when the fiber volume fraction respects the condition $\rho_f > \rho_{f,cr}$. If the fiber content verifies the condition that $\rho_f < \rho_{f,cr}$ a single macro-crack and a localized failure mode is expected.

6.3 Comparison between theoretical proposal and experimental data

The results obtained by employing the theoretical proposal are performed with the aim to predict the crack spacing distances on strain-hardening FRCC tested in direct tension.

The considered analyses were referred to the main geometrical and material properties deduced by the experimental evidences reported in Kim (2009) and Rinaldi and Grimaldi (2006) of fibrous concrete having steel fibers with hooked-ends. The simulations deal with four specimens characterized by different fiber contents ranging between 1.0% to 5.0%.

A linear decreasing stress-crack opening relation $\sigma_{cr} - \bar{u}_{cr}$ was adopted for estimating the crack spacing l_{cs}^I and the critical fiber content $\rho_{f,cr}$

$$\sigma_{cr} = \chi_0 - h \cdot \bar{u}_{cr} \tag{32}$$

being h a constant negative softening modulus proposed by the CEB-FIP-90 (1993) code, which value can be experimental derived in notched concrete prisms tested under uniaxial tensions (de Oliveira e Sousa and Gettu, 1992).

The following expressions for l_{cs}^I and $\rho_{f,cr}$ are finally derived by introducing Eq. (32) in Eqs. (27) and (31)

$$\begin{cases} l_{cs}^I = 1.5 \dfrac{2\coth^{-1}\left(\frac{2k_E\rho_f}{\sqrt{\alpha_1} d_f h}\right)}{\sqrt{\alpha_1}} \\ \rho_{f,cr} = \dfrac{\frac{\sqrt{d_f} h \sqrt{d_f E_s h^2 + 4{E_c}^2 k_E}}{\sqrt{E_s}} + d_f h^2}{2E_c k_E} \end{cases} \tag{33}$$

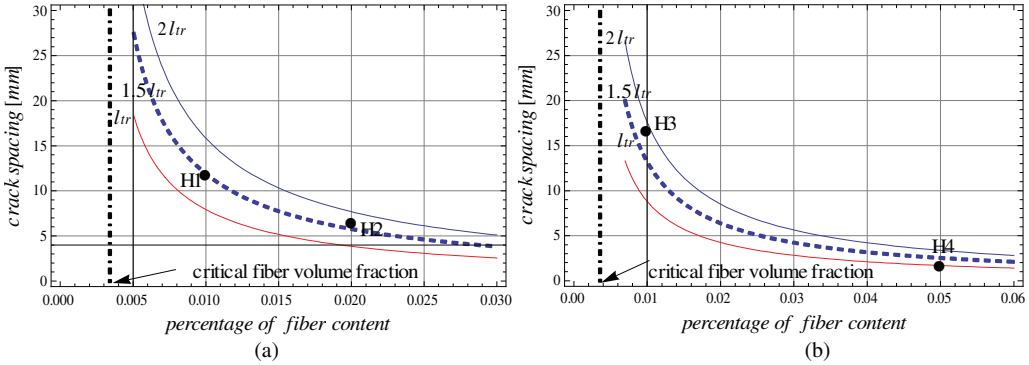

Figure 6: Crack spacing model results against experimental data on hooked-end steel fibers: (a) H1 and H2 by Kim (2009) and (b) H3 and H4 by Rinaldi and Grimaldi (2006).

The concrete and fiber proprieties are directly assumed on the bases of the experimental reports (Kim, 2009; Rinaldi and Grimaldi, 2006). Table 2 outlines the values of the relevant material parameters identified for the four experimental tests considered in the present section.

Table 2: Geometrical and material properties of the considered experimental FRCC specimens reinforced with hooked-end steel fibers: H1 and H2 by Kim (2009) and H3 and H4 by Rinaldi and Grimaldi (2006).

Test label	**Fibers**				**Concrete**		
	d_f [mm]	l_f [mm]	E_s [GPa]	ρ_f (%)	f_c [MPa]	χ_0 [MPa]	E_c [GPa]*
H1	0.38	30.0	200.0	1.0	84.0	4.2	43.7
H2	0.38	30.0	200.0	2.0	84.0	4.2	43.7
H3	0.56	30.0	200.0	1.0	25.0	0.1×f_c	36.5
H4	0.56	30.0	200.0	5.0	25.0	0.1×f_c	36.5

** Estimated value with the CEB-FIP Model Code 1990 formula*

The mechanical parameters (i.e., h and k_E) are identified for each considered experimental campaign: $h = 30\ N/mm^3$ is the value assumed in the theoretical proposal, while $k_E = 150\ N/mm^3$ and $k_E = 200\ N/mm^3$ are the bond stiffness for the H1-H2 and H3-H4 tests, respectively.

Fig. 6 proposes the comparison between the experimental results by Kim (2009) and Rinaldi and Grimaldi (2006) (dot symbols) and the corresponding numerical values (continuous and dashed lines) in terms of transmission lengths (l_{tr} or $2 \times l_{tr}$ given by the continuous curves) vs. fiber content, also by means of the crack spacings (dashed line) vs. percentage of fiber inclusions.

The proposed predictions and the experimental results confirm a very good capability and soundness of the model to predict the crack spacing in strain-hardening FRCC.

7 DOWEL EFFECT OF FIBERS CROSSING CONCRETE CRACKS

The dowel action resulting in a shear transfer mechanism represents an important component on the overall bridging effect of steel fibers in fracture processes of FRCC. A simple analytical model for reproducing the dowel action of fibers crossing cracks was developed. It is based upon the definition of both stiffness and strength of a generic fiber embedded in the concrete matrix and subjected to a transverse force.

The basis of the well-known Winkler beam theory is used to describe the dowel force, V_d,

corresponding to the transversal displacement, Δ. Its analytical solution is depicted as

$$V_d = E_s J_s \lambda_f^3 \Delta \tag{34}$$

where E_s is the steel elastic modulus and J_s the moment of inertia of fiber, while the transversal displacement is $\Delta = \|\varepsilon_{\mathbf{T}}\| \cdot l_f$. The Winkler parameter, λ_f, is analytically derived as

$$\lambda_f = \sqrt[4]{\frac{k_c d_f}{4 E_s J_s}} = \sqrt[4]{\frac{16 k_c}{E_s \pi d_f^3}} \tag{35}$$

being k_c the foundation stiffness (herein, the surrounding mortar) evaluated by means of the expression proposed by Bilal and El-Ariss (2007)

$$k_c = (127 \kappa_1 \sqrt{f_c}) / d_f^{\frac{2}{3}} \tag{36}$$

being f_c the concrete strength, d_f the fiber diameter and κ_1 a parameter to calibrate.

At last, the empirical expression proposed by Dulacska (1972) for RC-structures is taken as maximum dowel strength

$$V_{d,u} = k_{dow} d_f^2 \sqrt{|f_c||\sigma_{y,s}|} \tag{37}$$

where k_{dow} represents a non-dimensional coefficient to calibrate whose typical value 1.27 could be assumed as reference for RC-structures (Bilal and El-Ariss, 2007) while $\sigma_{y,s}$ is the steel strength.

Finally, the equivalent dowel stress to be considered in the composite model of Eq. (5) can be determined as follows

$$\tau_f = \frac{V_d}{A_f} \tag{38}$$

being A_f the cross fiber section.

8 NUMERICAL RESULTS AND COMPARISONS

Numerical predictions carried out in both plain and Steel Fiber Reinforced Concrete (SFRC) by adopting the microplane formulation are presented in this section. The comparisons between model predictions and the experimental data by Li and Li (2001) are reported in Fig. 7. The same set of experimental tests were already analyzed in Caggiano et al. (2011), where the stress-strain responses were mainly realized by using a novel interface model for FRCC proposed by the authors.

Table 3: Fiber types employed in the experimental tests by Li and Li (2001).

	Density $[g/cm^3]$	$d_f[mm]$	$l_f[mm]$	$\sigma_{y,s}[GPa]$	$E_s[GPa]$
Dramix type I	7.8	0.5	30	1.20	200
Dramix type II	7.8	0.5	50	1.20	200

The considered SFRC specimens contain two fiber types, namely "Dramix type I" and "type II" whose fundamental characteristics are given in Table 3. The model parameters of the proposed numerical analyses, adjusted according to the experimental data given in Li and Li (2001), result: $E_c = 39.5\,GPa$ and $\nu = 0.20$, $\tan\phi_0^{mic} = \tan\beta^{mic} = \tan\phi_r^{mic} = 0.6$,

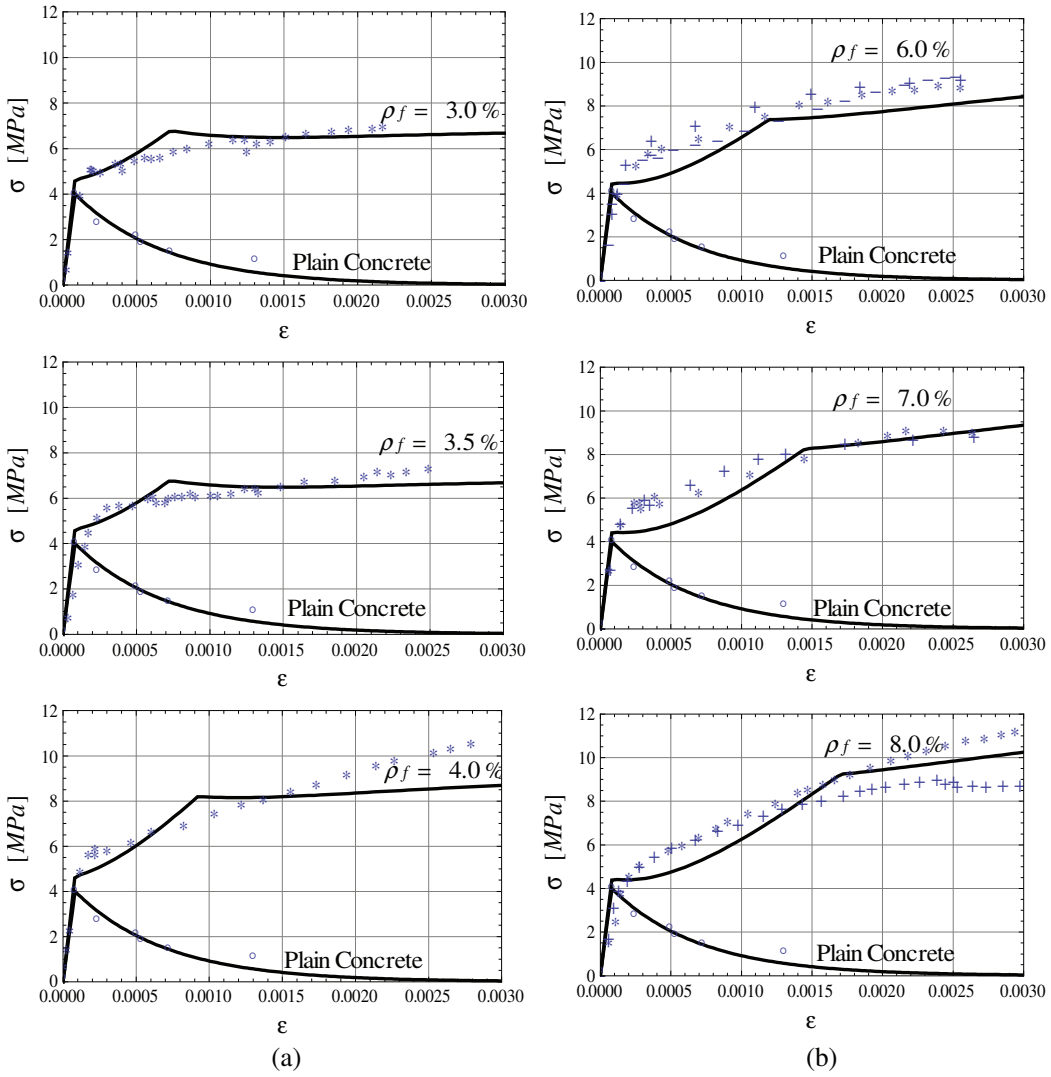

Figure 7: Comparison between the numerical predictions and the experimental results (discontinuous lines) by Li and Li (2001): (a) SFRC with "Dramix type II" and (b) SFRC with "Dramix type I".

$\chi_0^{mic} = 4.0\,MPa$, $c_0^{mic} = 7.0\,MPa$, $G_f^I = 0.12\,N/mm$, $G_f^{IIa} = 1.2\,N/mm$. While, the parameters of the fiber-to-concrete mechanisms are: $\tau_{y,a} = 1.70\,MPa$, $k_E = 105.00 MPa/mm$ and $k_S = 0.95 MPa/mm$ for the bond-slip strength; $\kappa_1 = 0.55$, $f_c = 10 \cdot \chi_0$ and $k_{dow} = 0.95$ for the dowel effect.

The stress-strain response for SFRCs with steel "Dramix type II", characterized by fiber contents ranging between 3.0% to 4.0%, are given in Fig. 7(a), while Fig. 7(b) depicts the numerical and experimental comparisons of SFRC tests characterized by "Dramix type I", whose fiber contents are 6.0%, 7.0% and 8.0%, respectively.

The numerical predictions compared against experimental results demonstrate a very good agreement. In fact, the model predicts in a very realistic mode the mechanical response of the analyzed SFRC specimens.

It is worth noting that all the numerical curves were obtained by just changing the fiber contents (ρ_f) and/or fiber types (e.g., l_f) according to the experimental reports. This aspect is the key advantage when the fiber effects are explicitly modeled, giving the possibility of modeling variation in the macroscopic stress-strain response by just changing the fiber type and

geometry.

9 CONCLUSIONS

The paper presented a microplane plasticity approach aimed at simulating the failure behavior of Fiber Reinforced Cementitious Composite (FRCC). It was based upon a macroscopic smeared-crack approach considering the failure of FRCC in a material point of view. The constitutive model considered the well-known "Mixture Theory" to simulate the combined bridging interactions of fibers in concrete cracks. The interactions between steel fibers and concrete matrix associated with bond-slip and dowel mechanisms were explicitly accounted in the constitutive formulation. The numerical simulations demonstrated that the constitutive proposal mainly captured the fundamental behaviors of FRCC. Very good agreement in terms of peak-strength and post-crack ductility was observed between numerical predictions and experimental results .

ACKNOWLEDGMENTS

The authors acknowledge the financial support for this work provided by CONICET (Argentine National Council for Science and Technology) through the Grant No. PIP 112-200801-00707, CIUNT (Research Council University of Tucuman) through the Grant No. E/26 479 and University of Buenos Aires through the Grant No. 20020090100 139. Moreover, the support to networking activities provided by "Encore" Project (FP7-PEOPLE-2011-IRSES n 295283; http://www.encore-fp7.unisa.it/) funded by the European Union within the Seventh Framework Programme is also gratefully acknowledged.

REFERENCES

Bazant Z. and Gambarova P. Crack shear in concrete: crack band microplane model. *ASCE J Struct Eng*, 110:2015–2035, 1984.

Bazant Z. and Oh B. Microplane model for progressive fracture of concrete and rock. *J Eng Mech ASCE*, 111(4):559–582, 1985.

Bazant Z. and Prat P. Microplane model for brittle plastic material: I. Theory. *J of Eng Mech*, 114(10):1672–1689, 1988a.

Bazant Z. and Prat P. Microplane model for brittle plastic material: II. Verification. *J of Eng Mech*, 114(10):1689–1703, 1988b.

Bazant Z., Tabbara M., Kazemi M., and Pijaudier-Cabot G. Random particle model for fracture of aggregate or fiber composites. *ASCE-J Eng Mech*, 116:1686–1705, 1990.

Beghini A., Bazant Z., Zhou Y., Gouirand O., and Caner F. Microplane model M5f for multiaxial behavior and fracture of fiber-reinforced concrete. *ASCE-J Mat Civil Eng*, 133(1):66–75, 2007.

Belytschko T., Lu Y., and Gu L. Crack propagation by element-free Galerkin methods. *Eng Fract Mech*, 51(2):295–315, 1995.

Bilal and El-Ariss. Behavior of beams with dowel action. *Eng Structures*, 29(6):899 – 903, 2007.

Caggiano A., Etse G., and Martinelli E. Interface model for fracture behaviour of fiber-reinforced cementitious composites (FRCCs): Theoretical formulation and applications. *European journal of environmental and civil engineering*, 15(9):1339–1359, 2011.

Caggiano A., Etse G., and Martinelli E. Zero-thickness interface model formulation for failure behavior of fiber-reinforced cementitious composites. *Computers & Structures*, 98-99(0):23 – 32, 2012a.

Caggiano A. and Martinelli E. A unified formulation for simulating the bond behaviour of fibres in cementitious materials. *Materials & Design*, 42(0):204 – 213, 2012.

Caggiano A., Martinelli E., and Faella C. A fully-analytical approach for modelling the response of frp plates bonded to a brittle substrate. *Int J of Solids and Structures*, 49(17):2291 – 2300, 2012b.

Carol I., Jirasek M., and Bazant Z. A thermodynamically consistent approach to microplane theory. Part I. Free energy and consistent microplane stresses. *Int J of Solids and Structures*, 38(17):2921 – 2931, 2001a.

Carol I., Lopez C., and Roa O. Micromechanical analysis of quasi-brittle materials using fracture-based interface elements. *Int J for Numerical Methods in Eng*, 52(1-2):193–215, 2001b.

Carol I., Prat P., and Lopez C. Normal/shear cracking model: Applications to discrete crack analysis. *ASCE-J Eng Mech*, 123:765–773, 1997.

CEB-FIP-90. *CEB, CEB-FIP Model Code 1990*. Bulletin d'information, Thomas Telford, London, pp. 203-205, 1993.

de Freitas J.T. and Cismasiu C. Hybrid-trefftz displacement element for spectral analysis of bounded and unbounded media. *Int J of Solids and Structures*, 40(3):671 – 699, 2003.

de Oliveira e Sousa J. and Gettu R. Determining the tensile stress-crack opening curve of concrete by inverse analysis. *ASCE - J Eng Mech*, 132(2):141–149, 1992.

di Prisco M., Plizzari G., and Vandewalle L. Fibre reinforced concrete: new design perspectives. *Materials and Structures*, 42:1261–1281, 2009.

Dulacska H. Dowel action of reinforcement crossing cracks in concrete. *ACI-Struct J.*, 69(12):754–757, 1972.

Dupont D. and Vandewalle L. *Calculation of Crack Widths with the $\sigma - \epsilon$ Method*. Test and Design Methods for Steel Fibre Reinforced Concrete: Background and Experiences - Proceedings of the RILEM TC162-TDF Workshop, RILEM Technical Committee 162-TDF, Bochum, Germany, pp. 119-144, 2003.

Etse G., Caggiano A., and Vrech S. Multiscale failure analysis of fiber reinforced concrete based on a discrete crack model. *Int J of Fracture*, pages 1–16, 2012. ISSN 0376-9429. 10.1007/s10704-012-9733-z.

Etse G. and Nieto M. Cosserat continua-based micro plane modelling. Theory and numerical analysis. *Latin American applied research*, 34:229 – 240, 2004.

Etse G., Nieto M., and Steinmann P. A micropolar microplane theory. *Int J of Eng Science*, 41(13-14):1631 – 1648, 2003.

Etse G. and Willam K. A fracture energy-based constitutive formulation for inelastic behavior of plain concrete. *ASCE-JEM*, 120:1983–2011, 1994.

Fantilli A., Ferretti D., Iori I., and Vallini P. Flexural deformability of reinforced concrete beams. *ASCE J Struct Eng*, 124(9):1041–1049, 1998.

Fantilli A., Mihashi H., and Vallini P. Multiple cracking and strain hardening in fiber-reinforced concrete under uniaxial tension. *Cement and Concrete Research*, 39(12):1217 – 1229, 2009.

Folino P. and Etse G. Performance dependent model for normal and high strength concretes. *Int J of Solids and Structures*, 49(5):701 – 719, 2012.

Kaczmarczyk L. and Pearce C.J. A corotational hybrid-Trefftz stress formulation for modelling cohesive cracks. *Computer Methods in Applied Mech and Eng*, 198(15-16):1298 – 1310, 2009.

Kim D. *Strain Rate Effect on High Performance Fiber Reinforced Cementitious Composites Using Slip Hardening High Strength Deformed Steel Fibers*. Ph.D. thesis, University of

Michigan, 2009.

Kuhl E. and Ramm E. Microplane modelling of cohesive frictional materials. *Europ. J Mech./A: Solids*, 19:121–143, 2000.

Kuhl E., Ramm E., and Willam K. Failure analysis of elasto-plastic material models on different levels of observation. *Int J of Solids and Structures*, 37(48-50):7259 – 7280, 2000.

Kuhl E., Steinmann P., and Carol I. A thermodynamically consistent approach to microplane theory. Part II. Dissipation and inelastic constitutive modeling. *Int J of Solids and Structures*, 38(17):2933 – 2952, 2001.

Li F. and Li Z. Continuum damage mechanics based modeling of fiber reinforced concrete in tension. *Int J Solids and Structures*, 38(5):777–793, 2001.

Li V. and Leung C. Steady-state and multiple cracking of short random fiber composites. *ASCE J Eng Mech*, 118(11):2246–2264, 1992.

Liu Z., Menouillard T., and Belytschko T. An XFEM/Spectral element method for dynamic crack propagation. *Int J of Fracture*, 169:183–198, 2011.

Meschke G. and Dumstorff P. Energy-based modeling of cohesive and cohesionless cracks via X-FEM. *Computer Methods in Applied Mech and Eng*, 196(21-24):2338 – 2357, 2007.

Nayal R. and Rasheed H. Tension stiffening model for concrete beams reinforced with steel and frp bars. *ASCE - J Mater. Civ. Eng*, 18(6):831–842, 1992.

Oliver J., Huespe A., and Sanchez P. A comparative study on finite elements for capturing strong discontinuities: E-FEM vs X-FEM. *Comput. Methods Appl. Mech Eng*, 195:4732–4752, 2006.

Oliver J., Linero D., Huespe A., and Manzoli O. Two-dimensional modeling of material failure in reinforced concrete by means of a continuum strong discontinuity approach. *Comput. Methods Appl. Mech Eng*, 197:332–348, 2008.

Rabczuk T. and Belytschko T. Application of particle methods to static fracture of reinforced concrete structures. *Int J of Fracture*, 137(1-4):19–49, 2006.

Rinaldi Z. and Grimaldi A. *Influence of high performance fiber reinforced concrete on the ductility of beam elements*. In Int Rilem Workshop on High performance Fiber Reinforced Cementitious Composites (HPFRCC) in Struct Applications, Rilem Publications SARL, Bagneux, 2006.

Sato Y. and Vecchio F. Tension stiffening and crack formation in reinforced concrete members with fiber-reinforced polymer sheets. *ASCE J Struct Eng*, 129(6):717–725, 2003.

Schauffert E. and Cusatis G. Lattice discrete particle model for fiber reinforced concrete (LDPM-F): I. theory. *J of Eng Mech*, 138(7):826–833, 2012.

Singh I., Mishra B., and Pant M. An enrichment based new criterion for the simulation of multiple interacting cracks using element free Galerkin method. *Int J of Fracture*, 167:157–171, 2011.

Trusdell C. and Toupin R. *The classical field theories*, volume III/I. Handbuch der Physik, Springer-Verlag, Berlin, 1960.

van Mier J., van Vliet M., and Wang T. Fracture mechanisms in particle composites: statistical aspects in lattice type analysis. *Mech of Materials*, 34:705–724, 2002.

Vrech S., Etse G., Meschke G., Caggiano A., and Martinelli E. Meso- and macroscopic models for fiber-reinforced concrete. In N. Bicanic, R. de Borst, H. Mang, and G. Meschke, editors, *Computational Modelling of Concrete Structures, Rohrmoos/Schladming, Austria*, pages 241–250. 2010.